


## RESEARCH ARTICLE

# Protein-imprinted particles for coronavirus capture from solution

Naomi L. Senehi<sup>1</sup>  | Matthew R. Ykema<sup>2</sup> | Ruonan Sun<sup>1</sup> | Rafael Verduzco<sup>3</sup> | Lauren B. Stadler<sup>1</sup> | Yizhi J. Tao<sup>2</sup> | Pedro J. J. Alvarez<sup>1</sup>

<sup>1</sup>Department of Civil and Environmental Engineering, Rice University, Houston, Texas, USA

<sup>2</sup>Department of Biosciences, Rice University, Houston, Texas, USA

<sup>3</sup>Department of Chemical and Biomolecular Engineering, Rice University, Houston, Texas, USA

## Correspondence

Department of Civil and Environmental Engineering, Rice University, Houston, TX, US, 77005, USA.

Email: [alvarez@rice.edu](mailto:alvarez@rice.edu)

Molecular imprinting is a promising strategy to selectively adsorb viruses, but it requires discerning and validating epitopes that serve as effective imprinting templates. In this work, glycoprotein-imprinted particles were synthesized for coronavirus capture. Adsorption was maximized at pH 6 (the glycoprotein isoelectric point) where the glycoprotein-imprinted particles outperformed non-imprinted particles, adsorbing  $4.96 \times 10^6 \pm 3.33 \times 10^3$  versus  $3.54 \times 10^6 \pm 1.39 \times 10^6$  median tissue culture infectious dose/mg of the target coronavirus, human coronavirus – organ culture 43, within the first 30 min ( $p = 0.012$ ). During competitive adsorption, with pH adjustment (pH 6), the glycoprotein-imprinted particles adsorbed more target virus than non-target coronavirus (human coronavirus – Netherland 63) with 2.34 versus 1.94 log removal in 90 min ( $p < 0.01$ ). In contrast, the non-imprinted particles showed no significant difference in target versus non-target virus removal. Electrostatic potential calculation shows that the human coronavirus – organ culture 43 glycoprotein has positively charged pockets at pH 6, which may facilitate adsorption at lower pH values. Therefore, tuning the target virus glycoprotein charge via pH adjustment enhanced adsorption by minimizing repulsive electrostatic interactions with the particles. Overall, these results highlight the effective use of glycoprotein-imprinted particles for coronavirus capture and discern the merits and limitations of glycoprotein imprinting for the capture of enveloped viruses.

## KEYWORDS

coronavirus, electrostatics, glycoprotein, molecular imprinting, silica

## Article Related Abbreviations:

APTES, (3-aminopropyl)triethoxysilane; FT-IR, Fourier-transform infrared spectroscopy; GIP, glycoprotein-imprinted particle; HCoV-NL63, human coronavirus – Netherland 63; HCoV-OC43, human coronavirus – Organ Culture 43; MIP, molecularly-imprinted particle; NIP, non-imprinted particle; PBS, phosphate-buffered saline; RT-qPCR, reverse transcription-quantitative polymerase chain reaction; SARS-CoV-2, severe acute respiratory syndrome coronavirus 2; TCID<sub>50</sub>, median tissue culture infectious dose.

## 1 | INTRODUCTION

Advances in the adsorptive separation of viruses from solution are critical for biomonitoring in numerous fields, including food production and safety, clinical diagnostics, and wastewater-based epidemiology. Methods used to concentrate viruses from solution often rely on size-exclusion (advanced filtration), electrostatic attraction (HA filtration), adsorption to salts (PEG precipitation),

or density sorting (ultracentrifugation). The sensitivity of subsequent quantification techniques, such as quantitative polymerase chain reaction and median tissue culture infectious dose (TCID<sub>50</sub>) assay, that follow virus separation depends on the efficiency of the virus concentration step [1]. However, these concentration methods lack specificity and thus do not selectively discern and separate the target from similar viruses. Furthermore, this non-specificity can lead to the co-concentration of analysis inhibitors and media components that hinder accurate quantification [2]. Thus, selective and specific methods for virus adsorption are needed, particularly for the removal and quantification of human pathogens such as severe acute respiratory syndrome coronavirus 2 (SARS-CoV-2) [3].

Molecularly-imprinted particles (MIPs) can impart selectivity and specificity to adsorptive virus separation methods [4–7]. During MIP preparation, a template molecule is embedded and then removed from a particle to create highly specific adsorption sites containing residual functional groups and shape complementarity that enhance adsorption. MIPs are typically centered around imprinting small molecules. However, surface imprinting strategies have been used to imprint macromolecular templates such as virus capsid proteins or whole viruses for whole virus capture [6, 8]. Notably, epitope imprinting of viral capsid protein was recently used to adsorb ~80% of a target virus (adenovirus type 5) and <10% of the non-target virus (minute virus of mice) when the blocking agent BSA was present [8]. This was accomplished using a non-enveloped virus as a target, with the off-target virus being another non-enveloped virus with significantly different capsid properties. In another study, up to 11 mutations out of 35 residues in a peptide template could effectively capture a non-mutated target protein peptide [9], which further highlights the potential use of moderately dissimilar proteins for templating selective and specific imprinted particles.

Macromolecular imprinting may enhance biosensing for coronavirus disease 2019 [10], but to our knowledge, most of these methods developed thus far have only imprinted and adsorbed dummy targets such as BSA [11], peptides [12, 16], and antigens [13, 14]. In the only case where SARS-CoV-2 glycoprotein was used as a MIP template for the development of a sensor, the absorption efficiency and specificity of the MIP for the target virion and other intact enveloped viruses were not systematically characterized [15].

Herein, we report glycoprotein-imprinted particles (GIPs) for the capture of human coronavirus – organ culture 43 (HCoV-OC43), a low pathogenicity virus with morphological and physiological similarities to SARS-CoV-2 [17]. For the analog non-target virus, we selected human coronavirus – Netherland 63 (HCoV-NL63), which

is also a low pathogenic human coronavirus that shares the same host receptor molecule (angiotensin-converting enzyme 2) as SARS-CoV-2 [17] and is commonly found in co-infection with HCoV-OC43 [18, 19]. Although HCoV-OC43 and HCoV-NL63 are similar in size (~75–125 nm) [20, 21] and morphology, the amino acid composition and charge property of their surface glycoproteins differ with an amino acid sequence identity of 38% [21, 22]. We show that the most pronounced difference between the HCoV-OC43 and HCoV-NL63 glycoproteins relevant to adsorption is their pH-dependent surface charge distribution, which allowed for moderately enhanced adsorption of the target virus (HCoV-OC43) to the GIPs at pH 6. However, even with pH adjustment, the selectivity and specificity of the GIPs for HCoV-OC43 over HCoV-NL63 were not outstanding, which highlights the need for a more selective separation strategy. Overall, this work advances our understanding of the merits and limitations of the unprecedented use of GIPs for enveloped virus adsorption.

## 2 | MATERIALS AND METHODS

### 2.1 | Materials

Phosphate-buffered saline (PBS), glutaraldehyde (25%), tetraethyl orthosilicate (TEOS, ≥99.0%), (3-aminopropyl)triethoxysilane (APTES), hydrochloric acid (HCl), and Triton X-100 were purchased from Millipore Sigma. All primers were purchased from Integrated DNA Technologies. The HCoV-OC43 Spike S1 Protein (His Tag) (> 90%) was purchased from Sino Biological. The iTaq Universal SYBR Green 1-Step Kit was purchased from Bio-Rad. HCoV-OC43 and BS-C-1 stocks were provided by Dr. Kui Li from the University of Tennessee Health Science Center, and HEK293T cells were provided in passage 3 from the Dr. Isaac Hilton lab at Rice University. HCoV-NL63 stocks were provided by BEI Resources.

### 2.2 | Preparation of viruses and template molecules

GIPs were synthesized using the S1 subunit of the HCoV-OC43 glycoprotein as the template molecule. The HCoV-OC43 S1 glycoprotein was diluted to a concentration of 0.05 μg/μl in 1X PBS, aliquoted, and stored at –80°C until use. For virus amplification, HEK293T cells were first grown to 50%–60% confluency in a T75 flask. Stock HCoV-OC43 was added at a multiplicity of infection of ~0.01, and media was added to a volume of 20 ml. Cells were grown in a 37°C incubator at 5% CO<sub>2</sub> for 5–6 days. At this time, cells

showed a full cytopathic effect. To remove virus particles from the cells, the flask went through 3 freeze/thaw cycles. The media was collected and spun down to remove cellular material at 500 x g for 5 min at 25°C. The media containing the virus was aliquoted and stored at -80°C. HCoV-NL63 stocks were prepared in the same way as the HCoV-OC43 but cultured in BS-C-1 cells. The virus propagation method was adapted from Leibowitz et al. 2011 [23].

### 2.3 | Synthesis of GIPs and non-imprinted particles

Due to their facile synthesis and adaptability to new templates, silica-based GIPs and non-imprinted particles (NIPs) were synthesized according to previous methods which were adapted for the HCoV-OC43 S1 glycoprotein template [6, 8, 24]. To a suspension of 4 mg silica/ml, 120 µl of 0.05 µg/µl glycoprotein was incubated for 1 h. TEOS (2 µl/mg silica) was first added and reacted for 2 h before lowering the water bath temperature to 10°C and reacting with APTES (0.4 µl/mg silica) for 1 h. The particles were washed once with water and cured for 24 h at 4°C. Finally, the particles were washed with clearing solution (HCl and Triton X-100) to remove the template and washed three times with 1X PBS before being oven dried at 40°C overnight. NIPs were produced in the same way with the omission of glycoprotein.

### 2.4 | Virus adsorption experiments

Adsorption experiments were conducted in 0.5X PBS adjusted to pH 6, 7.4, or 10. The pH of the PBS solutions was adjusted using either 1 M HCl (for pH < 7.4) or 0.1 M NaOH (pH > 7.4) dropwise. Then according to Equation (1), the ionic strength was adjusted using NaCl. For Equation (1),  $I$  is the ionic strength,  $c_i$  is the molar concentration of the ion,  $z_i$  is the charge of the ion, and  $n$  is the number of ions.

$$I = \frac{1}{2} \sum_{i=1}^n c_i z_i^2 \quad (1)$$

The GIPs or NIPs were resuspended by sonication into the adsorption buffer to a concentration of 5 mg/10 ml and magnetically stirred at 300 rpm throughout the experiment. At time zero 5 µl of the HCoV-OC43 stock solution (final concentration on the order of 10<sup>5</sup>-10<sup>6</sup> TCID<sub>50</sub>/ml) was added to each vial. Throughout the course of the experiment, 200 µl of the sample was taken at timepoints 0, 1, 2.5, 10, 30, 60, and 90 min. The samples were centrifuged at 8000 rpm for 1 min to settle the GIPs or NIPs and the supernatant was stored at 4°C until reverse

transcription-quantitative polymerase chain reaction (RT-qPCR) analysis. Positive virus controls were run for every experiment in which all conditions were followed as above without the addition of the GIPs or NIPs. For competitive adsorption, HCoV-OC43 and HCoV-NL63 were added in equal parts to a final concentration on the order of 10<sup>10</sup> TCID<sub>50</sub>/ml. Data are reported as log removal (Equation (2)) or adsorption capacity (Equation (3)), fitted using the least squares method to pseudo-second-order kinetics (Equation (4)), and validated using the Shapiro-Wilk test. In Equation (3) and Equation (4)  $q_t$  is the adsorption capacity at time  $t$ ,  $C_a$  is the concentration of the GIPs or NIPs,  $q_e$  is the equilibrium adsorption capacity and  $K$  is the adsorption rate constant. The theoretical adsorption density was calculated according to Equation (S1) where  $C_{spike}$  is the final concentration of the spiked virus in solution,  $SA$  is the surface area in m<sup>2</sup>/g, and  $C_a$  is the concentration of the GIPs or NIPs.

$$\text{Log Removal} = -\text{Log} \left( \frac{C_{\text{sample}}}{C_{0, \text{virus control}}} \right) \quad (2)$$

$$q_t = \frac{C_0 - C_t}{C_a} \quad (3)$$

$$q_t = \frac{t}{\left(\frac{1}{q_e}\right)t + \frac{1}{Kq_e^2}} \quad (4)$$

$$\text{Theoretical adsorption capacity} = \frac{C_{spike}}{SA * C_a} \quad (S1)$$

### 2.5 | Virus quantification

RT-qPCR was performed to quantify HCoV-OC43 (forward primer: 5'-ATGTCAATACCCCGGCTGAC-3', reverse: 5'-GGCTCTACTACGCGATCCTG-3') [25] and HCoV-NL63 (forward primer: 5'-GATAACCAGTCGAAGTCACCTAGTTC-3', reverse: 5'-ATTAGGAATCAATTCA-GCAAGCTGTG-3') [25] on a CFX96TM Real-Time System (Bio-Rad, USA) in 96-well plates. RNA was extracted by heating at 95°C for 5 min. Each RNA sample was run in triplicate with standard curves (virus diluted in 0.5X PBS) and no template controls on each plate. Negative controls (DNase&RNase-free DI water) were run in triplicate. The RT-qPCR mixture for each reaction contained 5 µl reaction mix (2x), 0.125 µl iScript reverse transcriptase, 1 µl forward and reverse mix primers (1 µM), and 3.875 µl template RNA to achieve a total volume of 10 µl. The cycle conditions used were: 50°C for 10 min, 95°C for 1 min 15 s followed by 40 cycles of 95°C for 15 s to anneal and extend before plate reading at 60°C for 30 s and a final melting curve to ensure that no nonspecific RT-qPCR products were generated. Cq values were converted to TCID<sub>50</sub> using

a standard curve where the virus concentration of the stock virus solution was measured using a traditional coronavirus TCID<sub>50</sub> assay [23].

## 2.6 | Virus and particle characterization

Intact HCoV-OC43 and HCoV-NL63 virions were imaged using TEM on a JEOL 1230 High Contrast. The GIPs and NIPs were visualized using environmental SEM (FEI Helios NanoLab 660 DualBeam) at a magnification of 80 000X and a voltage of 1 kV. Particles were pressed into conductive tape prior to imaging to increase sample conductivity. The zeta potential of the virion and particles were measured in 0.5X PBS on a Zetasizer Nano (Malvern Zen 3600). For these measurements, 1.8 mg of particle or 10<sup>5</sup> TCID<sub>50</sub>/ml of the virus was sonicated for 5 min in 10 ml of solution (either PBS at pH 6, 7.4, or 10) prior to measurement. The specific surface area and pore characteristics of the GIPs and NIPs were measured on a Quantachrome Autosorb-iQ-MP/KR BET Surface Analyzer and fit to the Brunauer–Emmett–Teller method and Barret, Joyner, Halenda method, respectively. The particle infrared spectra were measured via Fourier-transform infrared (FT-IR) spectroscopy on a diamond plate (Nicolet).

## 2.7 | Protein modeling

PyMOL was used for protein modeling of the HCoV-OC43 S glycoprotein (PDB: 6OHW) and HCoV-NL63 S glycoprotein (PDB: 7KIP). Electrostatic analysis at varying pH values (6, 7.4, and 10) was done through the APBS Electrostatics plugin [26]. Blue to red regions varies from +5kT to −5kT.

## 2.8 | Statistical analysis

For each adsorption experiment, three individual batches of particles (GIP or NIP) were tested independently. Results from individual runs were averaged and were found to be statistically significant at a 95% confidence interval using two-way analysis of variance ( $p < 0.05$ ). Data were fit using the least squares method and the Shapiro-Wilk test.

## 3 | RESULTS AND DISCUSSION

### 3.1 | Synthesis of coronavirus GIPs

The main goal of glycoprotein imprinting was to impart selectivity on an adsorbent (SiO<sub>2</sub>) for binding HCoV-OC43

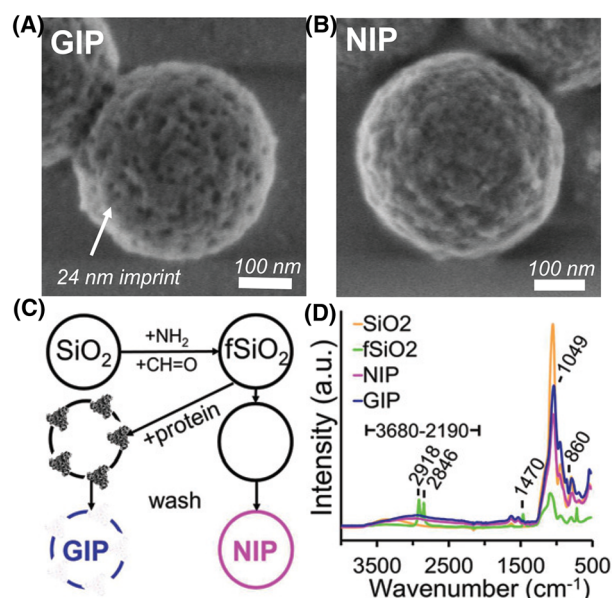


**FIGURE 1** SEM images of the (A) glycoprotein-imprinted particle (GIP) and (B) non-imprinted particle (NIP). (C) Schematic of the imprinting process and (D) corresponding FT-IR

virions in solution. Glycoprotein imprinting circumvents the use of pathogenic viruses as imprinting templates, and instead uses a template that is commercially available at a high purity, which can enhance reproducibility and bulk synthesis. The glycoprotein-imprinted silica-based particles (GIPs) were synthesized using the S1 subunit of the HCoV-OC43 glycoprotein (HCoV-OC43 S1 glycoprotein) as the template molecule as shown by SEM (Figure 1A). The NIP (Figure 1B) exhibited a relatively smooth surface compared to that of the GIP which showed small imprints that matched the size of the templated HCoV-OC43 S1 glycoproteins (Figure S1), on the order of 10 nm. The NIP and GIP had similar specific surface areas of ~14 m<sup>2</sup>/g (Table S1), yielding the same theoretical adsorption density (Equation (S1)) for the HCoV-OC43 virions (i.e.,  $6.93 \times 10^7$  TCID<sub>50</sub>/m<sup>2</sup>). The pore characteristics (Table S2) show that the NIP and GIP had an average pore diameter of ~3.96 nm and were mesoporous (pore sizes between 2 and 50 nm). This implies that the 75–125 nm diameter virions would bind to the surface of the particles, where the imprints are located, rather than within the pores of the material. Therefore, GIP and NIP performances can be compared to discern the effects of the surface imprints on specific and selective adsorption, without confounding effects of differences in surface area or pore characteristics of the particles.

The synthesis of these GIPs and NIPs was achieved via the imprinting process outlined in Figure 1C, and the successful progression of the imprinting process was further confirmed by FT-IR (Figure 1D). First, the SiO<sub>2</sub> was functionalized using APTES and crosslinker glutaraldehyde to

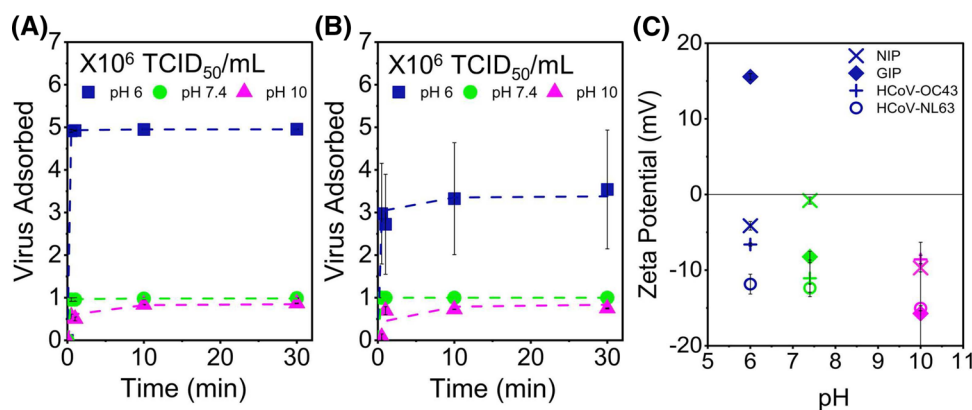


**FIGURE 2** The adsorption capacities of human coronavirus – organ culture 43 (HCoV-OC43) for the (A) glycoprotein-imprinted particle (GIP) and (B) non-imprinted particle (NIP) at different solution pH values. (C) Zeta-potential measurements of the polymers and viruses

create a functional layer (fSiO<sub>2</sub>) that anchored the HCoV-OC43 S1 glycoprotein to the surface before polymerizing around the glycoprotein. This is observed in the FT-IR spectra where the bare SiO<sub>2</sub> exhibits peaks at 1049 cm<sup>-1</sup> and an -OH stretch across 3680–2190 cm<sup>-1</sup> while the fSiO<sub>2</sub> shows functional peaks at 1470, 2918, and 2846 cm<sup>-1</sup>, and a reduced peak at 1049 cm<sup>-1</sup>. Imprints were created by washing the glycoprotein off the particles to produce GIPs, and the same procedure was conducted in the absence of glycoprotein to produce NIPs. The resulting GIP and NIP showed similar peaks for SiO<sub>2</sub> (1049 cm<sup>-1</sup>) and an -OH stretch (3680–2190 cm<sup>-1</sup>). The GIP showed a distinct peak at 860 cm<sup>-1</sup> in the fingerprint region and had a higher intensity. Thus, the FT-IR spectra corroborate the successful imprinting of the HCoV-OC43 S1 glycoprotein into the particles.

### 3.2 | Selective coronavirus adsorption to the GIPs was maximized at pH 6

The use of GIPs in environmental applications requires adsorption to be rapid and performed across a wide pH range; thus, adsorption kinetic studies were conducted at three pH values (6, 7.4, and 10) for up to 30 min. The best selectivity was achieved when the solution pH was adjusted to a value of 6, which is near the pI of the HCoV-OC43 S glycoprotein (5.52), as this minimizes electrostatic repulsion between the particles and virion (see surface charge measurements in the next section). At pH 6 the GIPs adsorbed a significantly greater ( $p < 0.05$ ) number of HCoV-OC43 virions than the NIPs as shown in Figure 2. Additionally, the GIPs reached an adsorption capacity of  $4.96 \times 10^6 \pm 3.33 \times 10^3$  TCID<sub>50</sub>/mg in less than 10 min ( $k = 4.93 \times 10^{-5}$  TCID<sub>50</sub> mg<sup>-1</sup> min<sup>-1</sup>). In comparison, the NIPs took 30 min to reach a lower adsorption capacity of  $3.54 \times 10^6 \pm 1.39 \times 10^6$  TCID<sub>50</sub>/mg. This selectivity was

not observed at pH 7.4 or pH 10 where the GIPs and NIPs adsorbed comparable amounts ( $\sim 7\text{--}9 \times 10^5$  TCID<sub>50</sub>/mg) of the HCoV-OC43 virions. In all cases, adsorption fit well with pseudo-second-order kinetics (Table 1), and an adsorption capacity  $> 10^5$  TCID<sub>50</sub>/mg was reached in under 30 min. This illustrates the potential use of the GIPs and NIPs in applications requiring rapid adsorption and the use of the GIPs in lower pH environments for selective virus capture.

The lack of selectivity at pH 7.4 and 10 suggest that electrostatic interactions overwhelmed any significant imprinting effect, underscoring the need to minimize electrostatic repulsion. Specifically, at pH 7.4 and 10 the virions and particles were both negatively charged ( $\leftarrow 8.58$  mV) (Figure 2C) and therefore likely to be repelled from one another. This was also the case at all pH values for the NIPs. In contrast, the zeta potential was positive for the GIPs at pH 6 (15.57 mV), which can facilitate adsorption via electrostatic attraction to the negatively charged HCoV-OC43 virions.

Differences in surface charge of the GIPs and NIPs at pH 6 and resulting adsorption behavior may be due to the residual functional group, shown as the 860 cm<sup>-1</sup> FT-IR peak in Figure 1, left behind on the GIPs after imprinting. To further elucidate the role of surface charge, the contribution of the glycoproteins to the negative charge of the HCoV-OC43 virion and subsequent adsorption behavior was assessed through protein modeling in PyMOL (Figure 3B–D). The simulations revealed that the HCoV-OC43 glycoprotein surface charge varies spatially with pH and becomes increasingly negative with increasing pH. This agrees with the adsorption kinetics behavior and zeta potential measurements. Therefore, although the particles and virus were in close range in all cases (zeta potentials between  $-20$  and  $20$  mV), electrostatic repulsions had to be minimized using pH adjustment to achieve selectivity using the GIPs.

TABLE 1 Fitting of the adsorption kinetics data to a pseudo-second-order model

	$k$ (TCID <sub>50</sub> mg <sup>-1</sup> min <sup>-1</sup> )			$q_e$ (TCID <sub>50</sub> /mg)			$R^2$		
	pH 6	pH 7.4	pH 10	pH 6	pH 7.4	pH 10	pH 6	pH 7.4	pH 10
GIP	4.93E-05	6.26E-05	2.87E-06	4.95E+06	9.84E+05	8.60E+05	1.00	1.00	0.96
NIP	2.67E-06	3.15E-03	1.30E-06	3.39E+06	1.00E+06	8.60E+05	0.98	1.00	0.78

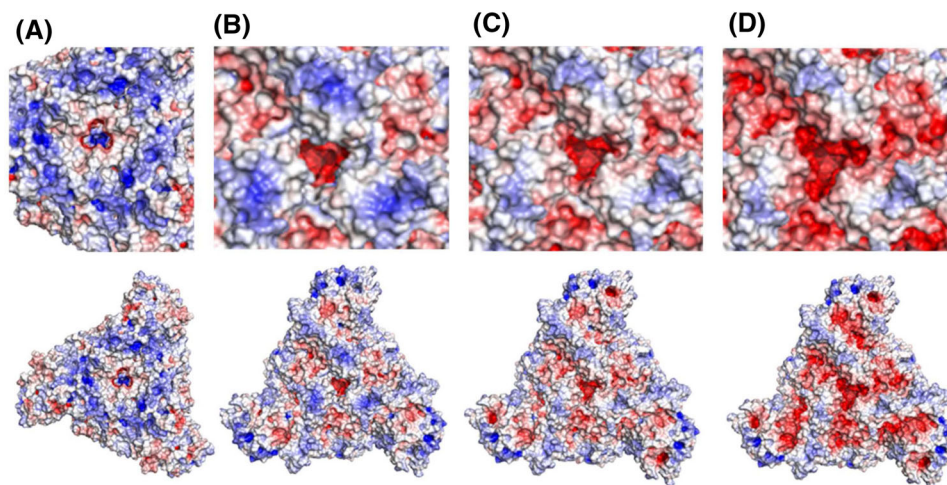


FIGURE 3 Protein modeling showing (A) surface charge of the human coronavirus – Netherland 63 (HCoV-NL63) S1 glycoprotein and (B) progression of the surface charge of the human coronavirus – organ culture 43 (HCoV-OC43) S1 glycoprotein at pH 6, (C) at pH 7.4, and (D) at pH 9.8. Blue to red regions vary from +5kT to -5kT

The overwhelming role of electrostatics, even once minimized by pH adjustment, has also been shown for perfluorooctanesulfonic acid adsorption to MIPs functionalized in a similar manner [27]. They attributed the adsorption of perfluorooctanesulfonic acid to the MIP/NIP largely to electrostatic interactions, instead of selective MIP binding, based on the decreasing adsorption at increasing pH [27]. Similarly, highly successful imprinted particles, such as adenovirus hexon protein imprinted particles [8], require the addition of blocking agents, such as BSA, to be selective. Therefore, our work corroborates and highlights that there is still a need for methods that enhance adsorption without relying on changes to the system such as pH adjustment or the addition of blocking agents.

### 3.3 | At pH 6 the GIPs enhance the removal of the target virus in the presence of two morphologically similar coronaviruses

To assess the specificity of the GIPs for only the target virus, adsorption of HCoV-OC43 from solution (at pH 6) in the presence of a competing virus (HCoV-NL63) was assessed. The GIPs adsorbed more HCoV-OC43 than HCoV-NL63 but were not highly selective. The GIPs removed 2.34-log (~99%) of HCoV-OC43 compared to 1.94-log (~90%) of

HCoV-NL63 ( $p < 0.01$ ) within 90 min (Figure 4). However, the NIPs also adsorbed about 2-log (99%) of the HCoV-OC43 and HCoV-NL63 virions within 90 min. This lack of selectivity (GIPs performing similarly to NIPs) and relatively slow adsorption time highlight the need for further optimization of the GIPs to be selective in the presence of similar (shape, size, charge, and so forth) viruses. However, the displayed specificity of the GIPs and not the NIPs for the target virus suggests the potential value of the GIPs when two or more viruses are co-occurring and should be separated, such as when diagnosing co-infections (e.g., HCoV-OC43 and HCoV-NL63) or distinguishing commingled environmental viruses (e.g., murine coronavirus and *Pseudomonas* virus phi 6).

The basis of molecular imprinting is shape recognition, which plays a major role in adsorption to the GIPs. HCoV-OC43 and HCoV-NL63 are similar in morphology and size (~75–125 nm) [20, 21] (Figure S1), but HCoV-NL63 is coated with glycoproteins that have a larger mass and different pI values (Table 2). Thus, reduced adsorption of HCoV-NL63 to the GIPs may be due to its larger glycoprotein size and dissimilar configuration to the imprint which reduces shape recognition to the imprints. We found that the role of surface charge also played a prevalent role in adsorption and selectivity, as shown in other works [28]. In the medium tested (0.5X PBS, pH 6) both viruses had an overall negative surface charge (Figure 2C) but

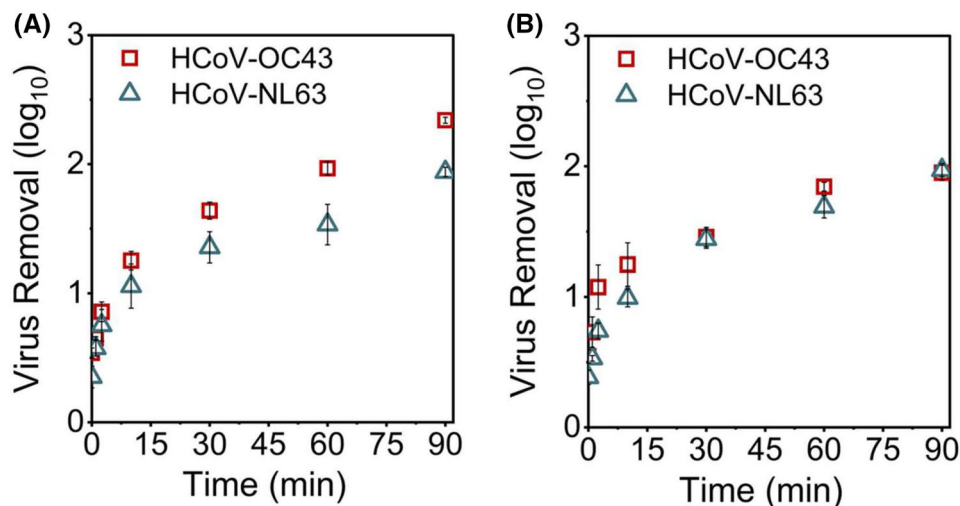


**FIGURE 4** Adsorption of human coronavirus – organ culture 43 (HCoV-OC43) and human coronavirus – Netherland 63 (HCoV-NL63) in a mixed virus solution to (A) the glycoprotein-imprinted particles (GIPs) or (B) non-imprinted particles (NIPs)

**TABLE 2** Virus and protein characteristics of the target and analog viruses used

	Target virus	Analog virus
	HCoV-OC43	HCoV-NL63
Virus Shape	spherical	spherical
Enveloped	Y	Y
Virus Diameter (nm)	125	75-155
Protein IEP	5.52 <sup>a</sup>	6.29 <sup>b</sup>
Protein Mass (Da)	81984	149850

<sup>a</sup>Isoelectric point of the HCoV-OC43 spike glycoprotein (GenBank ID: QQY99210.1)

<sup>b</sup>Isoelectric point of the HCoV-NL63 spike glycoprotein (GenBank ID: YP\_003767.1)

different surface charge distributions on their glycoproteins (Figure 3A,B), which may also lead to the observed differences in adsorption behavior. At pH 6, both HCoV-OC43 and HCoV-NL63 had widespread negatively charged regions that can facilitate adsorption based on the glycoprotein conformation during adsorption. However, the HCoV-OC43 glycoproteins had negatively charged edges that may be more accessible for adsorption to the particles, and lead to enhanced adsorption as compared to HCoV-NL63. It is important to note that the negative charge of the virions stems from all components on the surface including glycoproteins and exposed phospholipids; therefore, complex molecular interactions are at play when considering enveloped virus adsorption to MIPs.

Additional surface features of the virions apart from the glycoprotein have implications when designing imprinted particles for enveloped viruses. For example, for SARS-CoV-2, which is a homolog of HCoV-OC43, there is a low density of glycoproteins, with approximately one S protein

trimer per 1000 nm<sup>2</sup> of membrane surface [29]. Therefore, exposed phospholipids may play a large role in adsorption and serve as good imprinting templates to separate SARS-CoV-2 from non-enveloped viruses. On the other hand, the influenza A virus has a higher glycoprotein density with approximately one HA protein trimer per 100 nm<sup>2</sup> [30] and may be adsorbed well using GIPs with HA as an imprinting template. Although beyond the scope of the experimental and modeling aspects of this work, elucidating the specific binding events between the glycoprotein imprint and the diverse surface features of the target virion could help determine which features are good candidates for imprinting templates that can impart selectivity to enveloped viruses and therefore enhance adsorption. It is important to note that imprinting using intact enveloped viruses, rather than selected surface features, is probably impractical in most cases due to the large particle size and polymorphic shape of these viruses.

## 4 | CONCLUDING REMARKS

This work illustrates the merits of macromolecular imprinting for the adsorptive removal of two coronaviruses and the limitations in the selectivity and specificity of the particles when pH adjustment was not employed. This latter limitation of using functionalized silica for molecular imprinting is due to the inherent non-specificity of the material, which contains non-selective hydroxyl and amine groups. Whether future improvements in selectivity could be made by incorporating organosilanes with additional functional groups specific to the target virus protein [6] remains to be determined. Nevertheless, the advantage of molecular imprinting in capturing two coronaviruses

(HCoV-OC43 and HCoV-NL63) with high affinity was evident by fast removal (within 30 min) and an adsorption capacity  $\sim 10^6$  TCID<sub>50</sub>/mg when the pH was adjusted near the HCoV-OC43 S1 glycoprotein isoelectric point.

Although certain attributes such as the surface charge of the glycoprotein may enhance target-coronavirus adsorption when repulsive electrostatic interactions are suppressed, the specific adsorption mechanisms within the imprint, such as which pockets of the glycoprotein are adsorbing to functional groups within the imprint, need to be further elucidated. Developing a comprehensive understanding of the role of surface glycoproteins in adsorption will help enhance the design of imprinted materials that could be applied to physical separation methods, such as filtration, to selectively separate co-occurring and similarly shaped enveloped viruses, especially of public health importance such as SARS-CoV-2, HCoV-OC43, HCoV-NL63, Ebola, and human immunodeficiency virus.

To retrieve and reuse or analyze the SiO<sub>2</sub> particles, a process such as centrifugation, filtration or magnetic separation would be required. The latter could be enabled by imparting superparamagnetism, as previously demonstrated for proteins [31]. Once an appropriate particle separation method is selected, MIPs could also be used as a pretreatment or concentration step to enhance the sensitivity of subsequent quantification methods that play a vital role in biomonitoring for food safety, disease control, and wastewater-based epidemiology.

## ACKNOWLEDGMENTS

We would like to thank NSF (RAPID 2029339), DARPA (HR00112190062), Welch (C-1565), and the NSF Nanosystems Engineering Research Center for Nanotechnology-Enabled Water Treatment (ERC-1449500) for funding this project. Additional thanks go to Dongyang Zhu for running surface characteristic analysis, Hua Guo for particle imaging, and Cam Macisaac for assistance with FT-IR interpretation.

## CONFLICT OF INTEREST

The authors declare that they have no conflict of interest.

## DATA AVAILABILITY STATEMENT

Data are available on request from the authors.

## ORCID

Naomi L. Senehi  <https://orcid.org/0000-0002-5137-5721>

## REFERENCES

1. Corpuz M, Buonerba A, Vigliotta G, Zarra T, Ballesteros Jr F, Campiglia P, Belgiorio V, Korshin G, Naddeo V. Viruses in wastewater: occurrence, abundance and detection methods. *Sci Total Environ.* 2020;745:140910.
2. Ijzerman MM, Dahling DR, Fout GS. A method to remove environmental inhibitors prior to the detection of waterborne enteric viruses by reverse transcription-polymerase chain reaction. *J Virol Methods.* 1997;63:145–53.
3. Vitek R, do Nascimento FH, Masini JC. Polymer monoliths for the concentration of viruses from environmental waters: a review. *J Sep Sci.* 2022;45:134–48.
4. Altintas Z, Gittens M, Guerreiro A, Thompson K-A, Walker J, Piletsky S, Tothill IE. Detection of waterborne viruses using high affinity molecularly imprinted polymers. *Anal Chem.* 2015;87:6801–7.
5. Li N, Liu Y-J, Liu F, Luo M-F, Wan Y-C, Huang Z, Liao Q, Mei F-S, Wang Z-C, Jin A-Y. Bio-inspired virus imprinted polymer for prevention of viral infections. *Acta Biomaterialia.* 2017;51:175–83.
6. Cumbo A, Lorber B, Corvini PF-X, Meier W, Shahgaldian P. A synthetic nanomaterial for virus recognition produced by surface imprinting. *Nat Commun.* 2013;4:1–7.
7. Bolisay LD, Culver JN, Kofinas P. Optimization of virus imprinting methods to improve selectivity and reduce nonspecific binding. *Biomacromolecules* 2007;8:3893–9.
8. Gast M, Sobek H, Mizaikoff B. Selective virus capture via hexon imprinting. *Mater Sci Eng C.* 2019;99:1099–104.
9. Lu C-H, Zhang Y, Tang S-F, Fang Z-B, Yang H-H, Chen X, Chen G-N. Sensing HIV-related protein using epitope imprinted hydrophilic polymer coated quartz crystal microbalance. *Biosens Bioelectr.* 2012;31:439–44.
10. Laghrib F, Saqrane S, El Bouabi Y, Farahi A, Bakasse M, Lahrach S, El Mohammedi M. Current progress on COVID-19 related to biosensing technologies: new opportunity for detection and monitoring of viruses. *Microchem J.* 2021;160:105606.
11. Cennamo N, D'Agostino G, Perri C, Arcadio F, Chiaretti G, Parisio EM, Camarlinghi G, Vettori C, Di Marzo F, Cennamo R. Proof of concept for a quick and highly sensitive on-site detection of SARS-CoV-2 by plasmonic optical fibers and molecularly imprinted polymers. *Sensors* 2021;21:1681.
12. Fresco-Cala B, Rajpal S, Rudolf T, Keitel B, Groß R, Münch J, Batista AD, Mizaikoff B. Development and characterization of magnetic SARS-CoV-2 peptide-imprinted polymers. *Nanomaterials* 2021;11:2985.
13. Raziq A, Kidakova A, Boroznjak R, Reut J, Öpik A, Syritski V. Development of a portable MIP-based electrochemical sensor for detection of SARS-CoV-2 antigen. *Biosens Bioelectr.* 2021;178:113029.
14. McClements J, Bar L, Singla P, Canfarotta F, Thomson A, Czulak J, Johnson RE, Crapnell RD, Banks CE, Payne B, Seyedin S, Losada-Pérez P, Peeters M. Molecularly imprinted polymer nanoparticles enable rapid, reliable, and robust point-of-care thermal detection of SARS-CoV-2. *ACS Sensors.* 2022;7:1122–31.
15. Ayankoji AG, Boroznjak R, Reut J, Öpik A, Syritski V. Molecularly imprinted polymer based electrochemical sensor for quantitative detection of SARS-CoV-2 spike protein. *Sens Actuators B Chem.* 2022;353:131160.
16. Bognár Z, Supala E, Yarman A, Zhang X, Bier FF, Scheller FW, Gyurcsányi RE. Peptide epitope-imprinted polymer microarrays for selective protein recognition. Application for SARS-CoV-2 RBD protein. *Chem Sci.* 2022;13:1263–9.
17. Hofmann H, Pyrc K, Van Der Hoek L, Geier M, Berkhout B, Pöhlmann S. Human coronavirus NL63 employs the severe acute respiratory syndrome coronavirus receptor for cellular entry. *Proc Natl Acad Sci.* 2005;102:7988–93.



18. Vabret A, Mourez T, Dina J, Van Der Hoek L, Gouarin S, Petitjean J, Brouard J, Freymuth F, Human coronavirus NL63, France. *Emerg Infect Dis.* 2005;11:1225.
19. Killerby ME, Biggs HM, Haynes A, Dahl RM, Mustaqim D, Gerber SI, Watson JT, Human coronavirus circulation in the United States 2014–2017. *J Clin Virol.* 2018;101:52–6.
20. Orenstein JM, Banach B, Baker SC, Morphogenesis of coronavirus HCoV-NL63 in cell culture: a transmission electron microscopic study. *Open Infect Dis J.* 2008;2:52–8.
21. Liu DX, Liang JQ, Fung TS, Human Coronavirus-229E, -OC43, -NL63, and -HKU1 (Coronaviridae). *Encycl Virol.* 2021, 428–40.
22. Reguera J, Mudgal G, Santiago C, Casasnovas JM, A structural view of coronavirus–receptor interactions. *Virus Res.* 2014;194:3–15.
23. Leibowitz J, Kaufman G, Liu P, Coronaviruses: propagation, quantification, storage, and construction of recombinant mouse hepatitis virus. *Curr Prot Microbiol.* 2011;21, 15E. 11.11–46.
24. Sykora S, Silica-based functional materials: recognition and detection of viruses. 2018.
25. Wan Z, Zhang Yn, He Z, Liu J, Lan K, Hu Y, Zhang C, A melting curve-based multiplex RT-qPCR assay for simultaneous detection of four human coronaviruses. *Int J Mol Sci.* 2016;17:1880.
26. Jurrus E, Engel D, Star K, Monson K, Brandi J, Felberg LE, Brookes DH, Wilson L, Chen J, Liles K, Chun M, Li P, Gohara DW, Dolinsky T, Konecny R, Koes DR, Nielsen JE, Head-Gordon T, Geng W, Krasny R, Wei G-W, Holst MJ, McCammon JA, Baker NA, Improvements to the APBS biomolecular solvation software suite. *Prot Sci.* 2018;27:112–28.
27. Yu Q, Deng S, Yu G, Selective removal of perfluorooctane sulfonate from aqueous solution using chitosan-based molecularly imprinted polymer adsorbents. *Water Res.* 2008;42:3089–97.
28. Li X, Zhou J, Tian L, Li W, Zhang B, Zhang H, Zhang Q, Bovine serum albumin surface imprinted polymer fabricated by surface grafting copolymerization on zinc oxide rods and its application for protein recognition. *J Sep Sci.* 2015;38:3477–86.
29. Ke Z, Oton J, Qu K, Cortese M, Zila V, McKeane L, Nakane T, Zivanov J, Neufeldt CJ, Cerikan B, Lu JM, Peukes J, Xiong X, Kräusslich H-G, Scheres SHW, Bartenschlager R, Briggs JAG, Structures and distributions of SARS-CoV-2 spike proteins on intact virions. *Nature* 2020;588:498–502.
30. Chlanda P, Mekhedov E, Waters H, Schwartz CL, Fischer ER, Ryham RJ, Cohen FS, Blank PS, Zimmerberg J, The hemifusion structure induced by influenza virus haemagglutinin is determined by physical properties of the target membranes. *Nat Microbiol.* 2016;1:16050.
31. Gao R, Zhao S, Hao Y, Zhang L, Cui X, Liu D, Zhang M, Tang Y, Synthesis of magnetic dual-template molecularly imprinted nanoparticles for the specific removal of two high-abundance proteins simultaneously in blood plasma. *J Sep Sci.* 2015;38:3914–20.

### SUPPORTING INFORMATION

Additional supporting information can be found online in the Supporting Information section at the end of this article.

**How to cite this article:** Senehi NL, Ykema MR, Sun R, Verduzco R, Stadler LB, Tao YJ, Alvarez PJJ. Protein-imprinted particles for coronavirus capture from solution. *J Sep Sci.* 2022;1–9.  
<https://doi.org/10.1002/jssc.202200543>